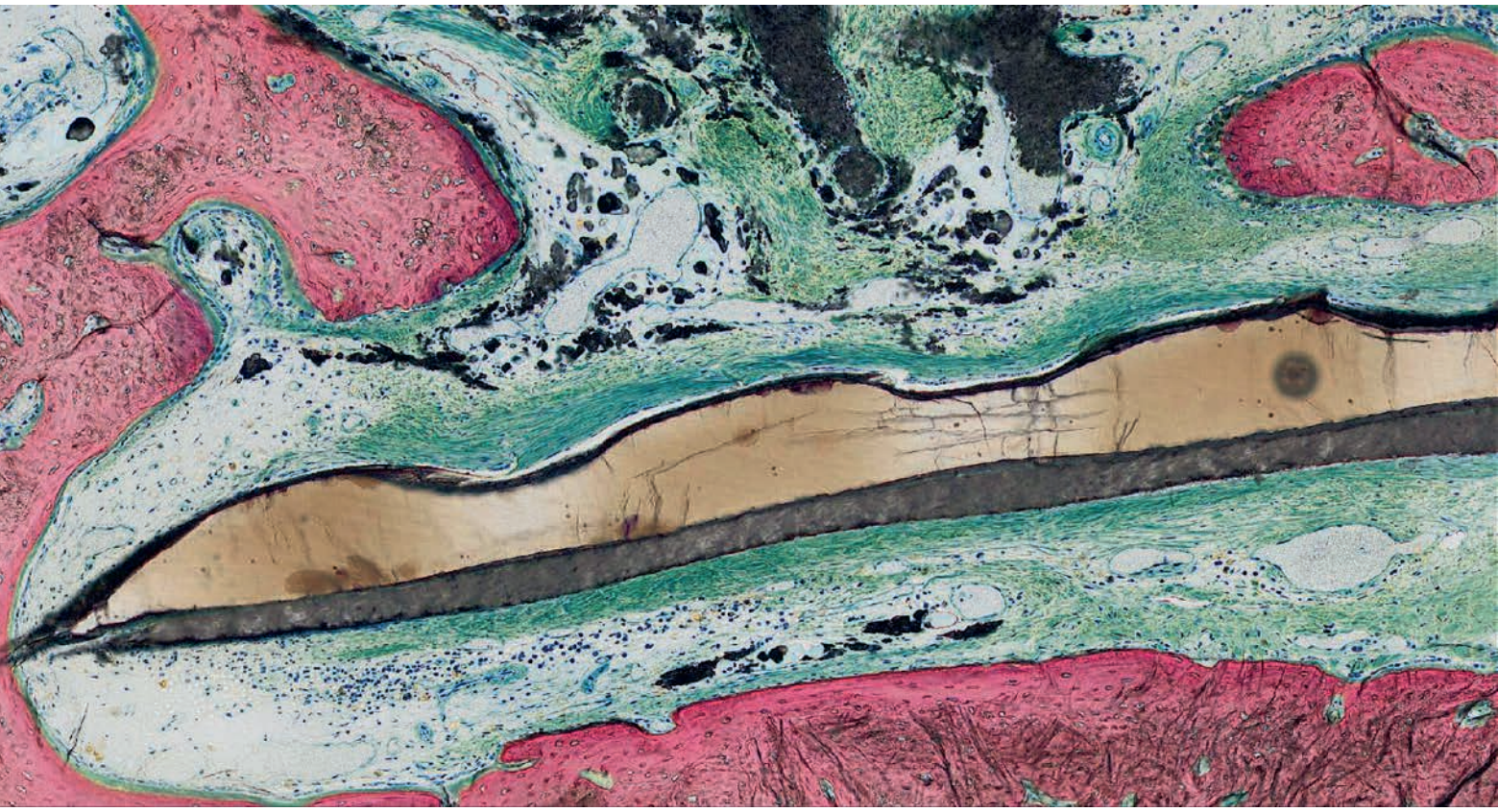

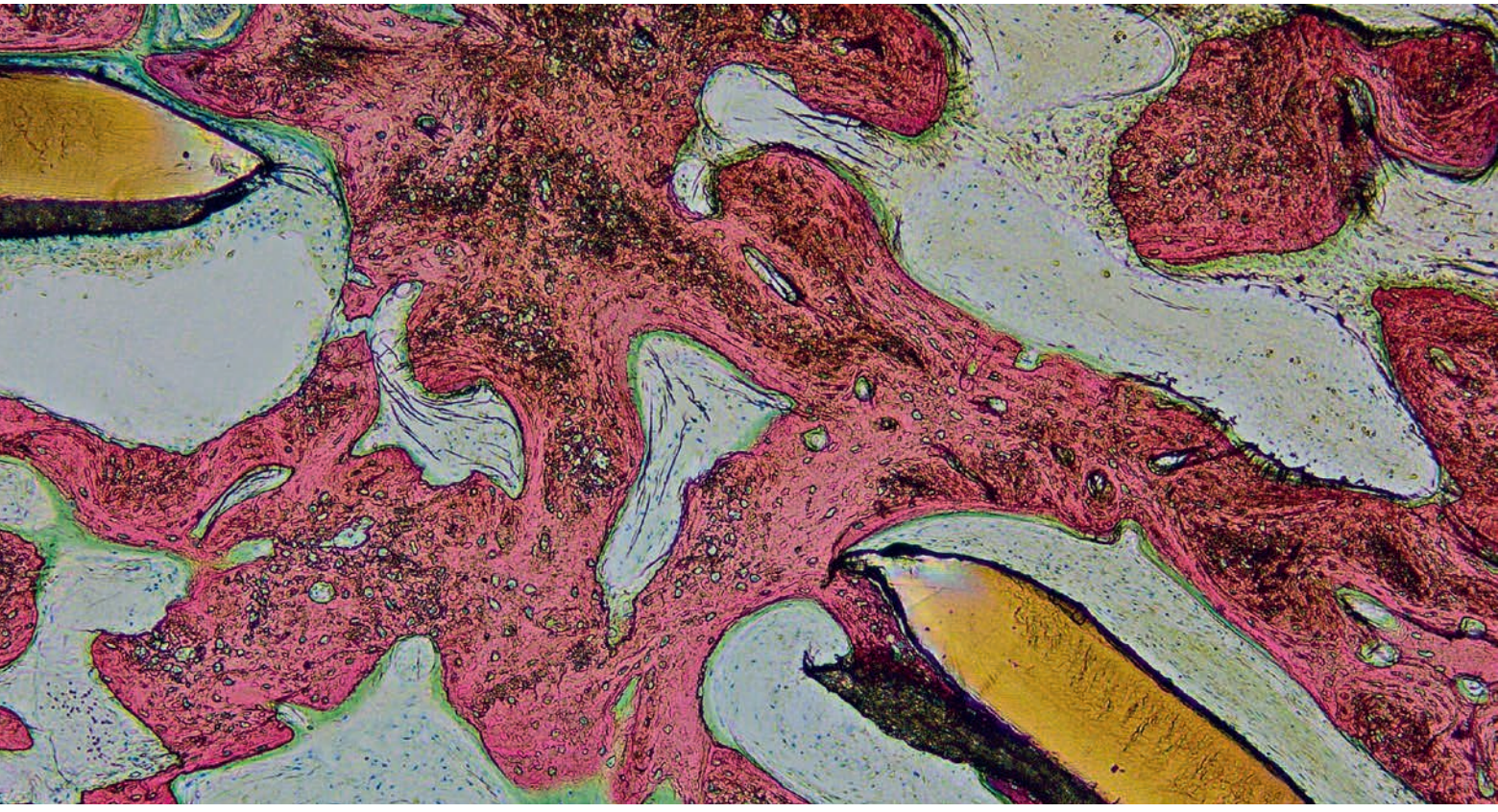

Submitted January 9, 2024;
accepted February 29, 2024.

Istvan A. Urban, DMD, MD, PhD
Nicholas Mirsky, BS
Matteo Serroni, DDS, MS
Nick Tovar, PhD, DDS
Vasudev Vivekanand Nayak, MSci, PhD
Lukasz Witek, MSci, PhD
Charles Marin, DDS, MS, PhD
Muhammad H. A. Saleh, BDS, MS, MSD
Andrea Ravidà, DDS, MS, PhD
Istvan Baczko, MD, PhD
Laszlo Parkanyi, DDS, PhD
Katalin Nagy, DDS, PhD
Paulo G. Coelho, MD, DDS, PhD, MBA

Elucidating the Benefit of Perforated vs Nonperforated Membranes in Guided Bone Regeneration: An In Vivo Histologic Evaluation and Histomorphometric Analysis

Nonperforated polytetrafluoroethylene (PTFE) membranes are effectively utilized in guided bone regeneration (GBR) but may hinder cell migration due to limited interaction with the periosteum. This study compared bone regeneration using occlusive or perforated membranes combined with acellular collagen sponge (ACS) and recombinant human bone morphogenetic protein-2 (rhBMP-2) in a canine mandibular model. Male Beagle dogs (n = 3) received two mandibular defects each to compare ACS/rhBMP-2 with experimental (perforated group) and control (nonperforated group) membranes (n = 3 defects/group). Tissue healing was assessed histomorphologically, histomorphometrically, and through volumetric reconstruction using microcomputed tomography. The perforated group showed increased bone formation and reduced soft tissue formation compared to the nonperforated group. For the primary outcome, histomorphometric analysis revealed significantly greater total regenerated bone in the perforated group (67.08% ± 6.86%) than the nonperforated group (25.18% ± 22.44%) (*P* = .036). Perforated membranes had less soft tissue infiltration (32.91% ± 6.86%) than nonperforated membranes (74.82% ± 22.44%) (*P* = .036). The increased permeability of membranes in the perforated group potentially enabled periosteal precursor cells to have greater access to rhBMP-2. The availability may have accelerated their differentiation into mature bone-forming cells, contributing to the stimulation of new bone production relative to the nonperforated group. *Int J Periodontics Restorative Dent 2025;45:341–355. doi: 10.11607/prd.7110*

Keywords: *bone regeneration, implants, osteogenesis, periosteum, polytetrafluoroethylene*

Guided bone regeneration (GBR) is a well-established surgical technique that aims to regenerate bone in critical defects to enable sufficient bone mass for implant placement.[1–5] This technique operates on the principle of compartmentalization, which is achieved through the use of barrier membranes.[6] This approach, based on results from experimental, preclinical animal studies, aims to protect the regenerating area via a physical barrier that mechanically

impedes soft tissue invagination into the osseous defect while simultaneously ensuring blood clot stabilization.[7,8] According to Wang and Boyapati,[9] effective GBR depends on four principles: *(1)* achieving primary closure of the surgical site to facilitate healing; *(2)* ensuring adequate blood supply, which delivers essential nutrients and growth factors that are critical for regeneration; *(3)* maintaining blood clot stability at the surgical site; and *(4)* creating and preserving a defined space that facilitates the colonization and differentiation of osteoprogenitor cells. This structured space is crucial for the successful regeneration of bone tissue.

A variety of resorbable and nonresorbable membranes have been utilized to achieve successful GBR outcomes. Notably, nonperforated polytetrafluoroethylene (PTFE) membranes (expanded, high density, and titanium-reinforced variants) have traditionally been favored due to their biocompatibility and effectiveness in maintaining space and providing occlusive action.[10,11] However, the significance of membrane porosity in GBR has been a subject of extensive research, yielding noteworthy results.[8,12–15] For example, occlusive properties of nonporous membranes inhibit the migration of epithelial and fibroblastic cells into the regenerative area. This lack of porosity may limit interaction with the periosteum and revascularization from the surgically elevated flap, which are critical for successful bone regeneration.[16] As such, membrane porosity has the potential to improve GBR outcomes by maintaining an appropriate balance between gingival soft tissue exclusion properties and maintaining available permeability for mesenchymal cells, biologic regulatory factors, and nutrients from outside the membrane.[17–20]

The evolution of research has led to a growing focus on the physiology and biology of the periosteum and its integral role in bone regeneration.[21] Several studies have underscored the periosteum's unique contribution to the healing of bone fractures.[22–24] The activation of periosteal-derived mesenchymal progenitor cells has been shown to drive the acquisition of osteogenic and chondrogenic capacity, the inductive marker-mediated properties on angiogenesis, and, consequently, bone graft vascularization.[25,26] Notably, in vivo studies have suggested that the efficacy of recombinant human bone morphogenic protein-2 (rhBMP-2) in bone regeneration procedures requires the presence of a periosteum to exert the maximum therapeutic effect.[27,28] In fact, BMP, synthesized through the recombinant DNA technique, has been shown to induce clinically relevant bone formation in various applications in the craniofacial skeletons of animal models.[29,30]

Specifically, rhBMP-2 has demonstrated the highest osteoinductive potential of the BMP family. Studies have demonstrated that bone regeneration in defects treated with rhBMP-2 (with or without GBR membranes) progressed faster relative to GBR techniques that did not involve the use of rhBMP-2.[31–34] Therefore, the aim of this study was to conduct a histologic and histomorphometric analysis of bone regeneration in critical vertical defects. The evaluation was carried out by comparing the use of occlusive vs perforated membranes in conjunction with acellular collagen sponge (ACS) and rhBMP-2 in a canine mandibular model. This comparison aimed to elucidate the potential benefits and effectiveness of these techniques in clinical applications.

Materials and Methods

Study Design and Animals

Male beagle dogs (n = 3) weighing ~15 kg were acquired and treated using a split-mouth model. Each dog had two defect sites created within each subject, one on each side of the mandible, to compare treatment involving ACS/rhBMP-2 with an experimental membrane (perforated group) relative to ACS/rhBMP-2 with a control membrane (nonperforated group). The animals were selected in accordance with the following inclusion criteria: *(1)* presenting an intact mandible; *(2)* absence of general occlusal trauma; *(3)* absence of oral lesions of viral or fungal nature; and *(4)* having good general health without systemic conditions, as ascertained by a veterinary clinical examination.

The study was carried out at the Pharmacology Research Center at the University of Szeged School Medicine after receiving ethical committee approval from the Pest County government office

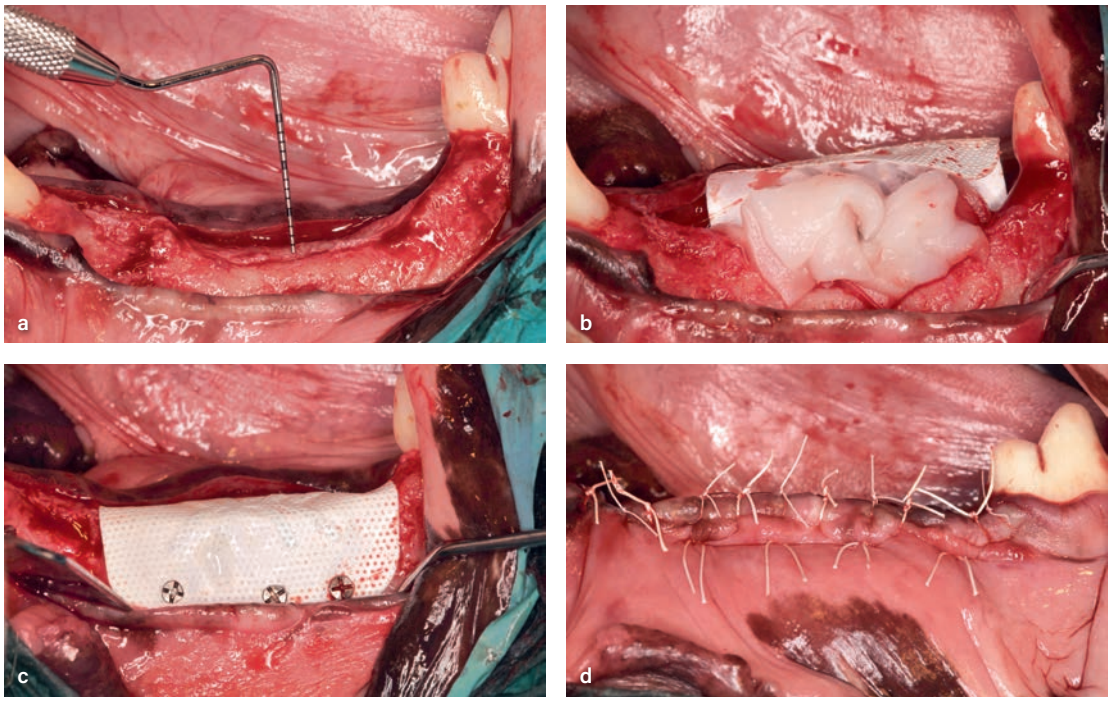

▲ **Fig 1** Nonperforated group. Overview of the surgical procedure performed after 8 weeks of healing. *(a)* Crestal incisions were made, and full-thickness lingual and buccal flaps were created on both sides of the mandible. *(b)* Nonperforated membranes and rhBMP-2/ACS were placed and subsequently trimmed to shape. *(c)* Titanium pins were used to secure the membranes. *(d)* After flap approximation, primary closure was achieved by the double-line suture technique with a nonabsorbable surgical suture.

(Pest Megyei Kormanyhivatal ethical permission no: CSI/01/487-4/2013) in accordance with the appropriate institutional and national guidelines for the adequate care of animals. Animals were housed individually during the acclimation period and subsequently cared for in specially designed kennels in a 12:12-hour light/dark cycle at 21°C to 22°C for the remainder of the in-life phase. Pelleted dog food (~300 g dry food) presoftened with water (~500 mL water added) was provided throughout the entire study period.

Surgical Procedures

The first stage of the study included the following surgical procedures: bilateral extraction of mandibular premolars (P1 to P4) and the first molars (M1). A midcrestal incision was made, and a full-thickness flap was raised to expose the mandibular bone. Teeth were extracted, and bilateral defects were created (~25 mm mesiodistally, ~8 mm apicocoronally, and ~10 mm buccolingually) using a low-speed cylindrical burr under copious irrigation. The flaps were repositioned and sutured in two layers utilizing 3-0 monofilament sutures.

After 8 weeks of healing, the animals were subjected to a follow-up surgical procedure. Figures 1 and 2 show the surgical steps of the nonperforated and perforated groups, respectively. During the follow-up procedure, a crestal incision was made from the distal surface of the canine to the distal surface of the first molar, enabling the creation of full-thickness lingual and buccal flaps on both sides of the mandible (see Figs 1a and 2a). Chronic vertical defects were emptied of remaining soft tissue, and perforations were made on the bone cortex to expose the underlying marrow bone. A 5-mm–long tenting screw was fixated to the remaining crest to standardize the augmentation on both sides of the mandible and to support the reinforced membranes. According to a split-mouth design, each animal received a Cytoplast Occlusive Titanium-Reinforced (TR) perforated membrane (Osteogenics Biomedical) and rhBMP-2/ACS (Infuse, Medtronic) on one side (see Fig 2b), and a Cytoplast Occlusive TR nonperforated

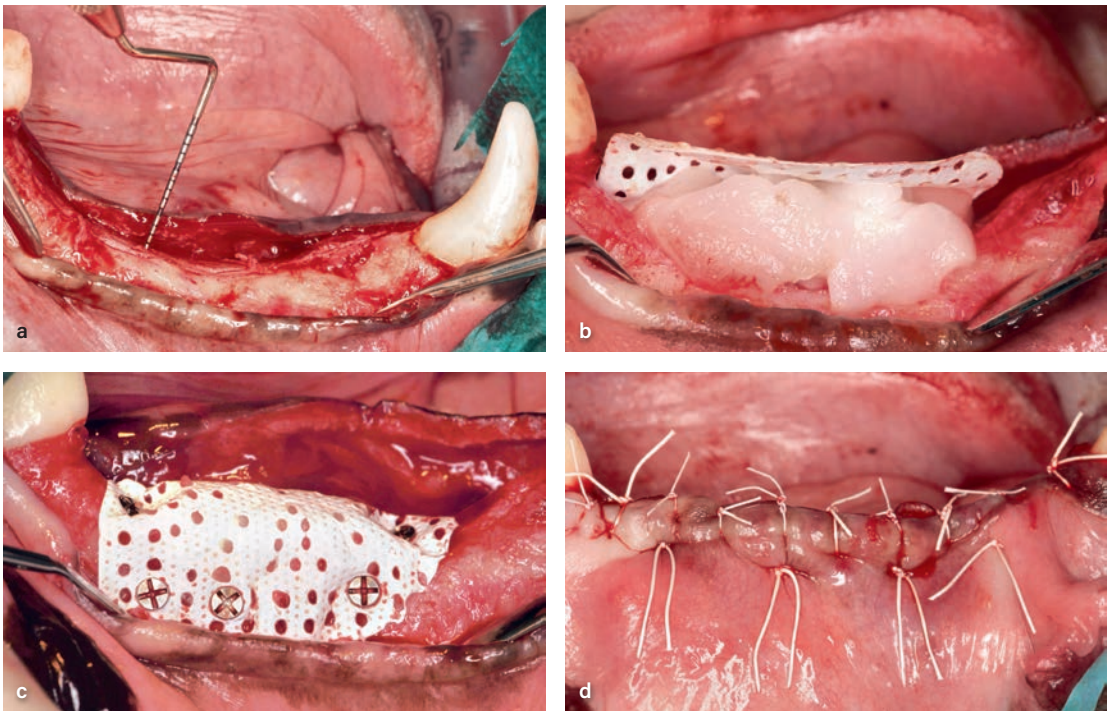

▲ **Fig 2** Perforated group. Overview of the surgical procedure performed after 8 weeks of healing. *(a)* Crestal incisions were made, and full-thickness lingual and buccal flaps were created on both sides of the mandible. *(b)* Perforated membranes and rhBMP-2/ACS were placed and subsequently trimmed to shape. *(c)* Titanium pins were used to secure the membranes. *(d)* After flap approximation, primary closure was achieved by the double-line suture technique with a nonabsorbable surgical suture.

membrane and rhBMP-2/ACS on the contralateral side (see Fig 1b). Pores were created in the membranes via a rubber dam punch (0.66 mm each, created by the membrane manufacturer). In both the perforated and nonperforated groups, the ACS was saturated with rhBMP-2 (0.2 mg/mL) prior to placement within the defect. Membranes were trimmed to shape and draped over the ridge so that the membranes completely covered the defects and extended beyond the margins by ~2 to 3 mm (see Figs 1c and 2c).

Titanium pins were used to secure the membrane (Master-Pin-Control Kit, Meisinger). The coronal advancement of the flap and its passive adaptation on the regenerated area was obtained by a horizontal periosteal incision and a "sweeping" motion. This technique is performed via lateral tension of the coronal segment, applying pressure with a blunt instrument in a sweeping motion, allowing the flap to stretch over the defect site for sufficient flap mobility and proper, tension-free approximation of the incision margins.[35] Primary closure was achieved by double-line suturing with a nonabsorbable surgical suture (Cytoplast PTFE, Osteogenics Biomedical). After flap approximation, the coronal portion of the membrane was interfaced with the intact periosteum, and in the apical region, the underlying connective tissue was in contact with the membrane (see Figs 1d and 2d).

Following both surgical procedures, animals were provided a soft diet. Sutures were removed 14 days postoperatively. Sites were evaluated three times per week, and the surgical wounds were disinfected with 0.12% chlorhexidine solution. After the first 14 days, healing was assessed weekly, and the remaining teeth were debrided monthly by supragingival scaling. Eight weeks after the second surgery, the animals were sedated and subsequently euthanized through overdose of thiopental (Trapanal, Abbott Laboratories). Each hemi-mandible was harvested, dissected, and fixed in 4% phosphate buffered formalin (pH = 7) for 10 days prior to further processing.

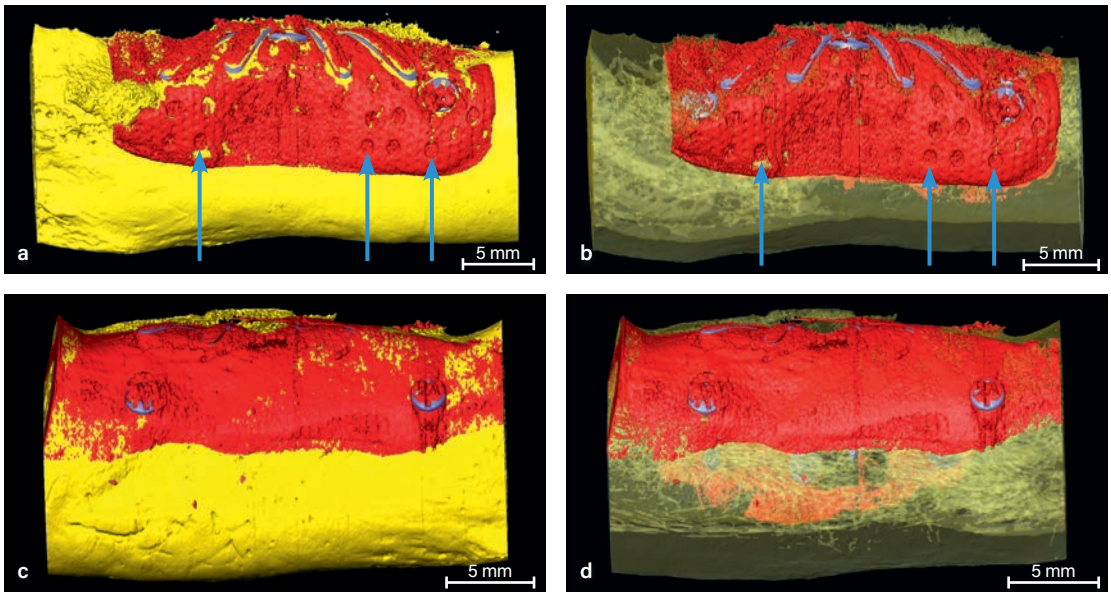

▲ **Fig 3** Representative volumetric reconstruction of the *(a and b)* perforated group and *(c and d)* nonperforated group. Bone *(yellow)* is shown in shaded *(a and c)* and translucent *(b and d)* views. The membrane is shown in *red*. Titanium fixation devices are shown in purple. *Arrows* in the perforated group identify the pores within the membranes. Images are oriented in the buccolingual direction.

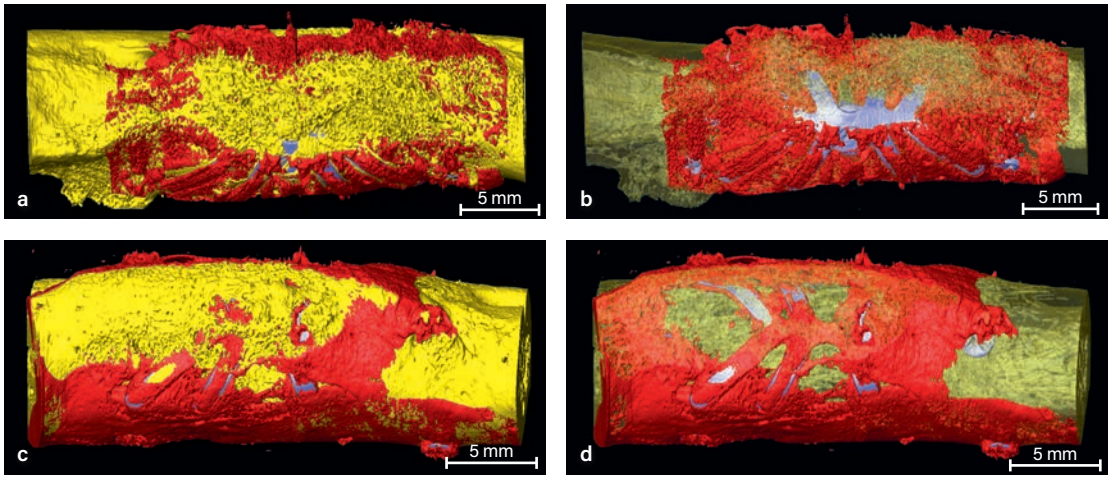

▲ **Fig 4** Representative volumetric reconstruction of the *(a and b)* perforated group and *(c and d)* nonperforated group. Bone *(yellow)* is shown in shaded *(a and c)* and translucent *(b and d)* views. The membrane is shown in *red.* Titanium fixation devices are shown in *purple*. Images are oriented in the superior-inferior direction.

Microtomographic Analysis

During the scanning phase, samples were submerged in a 70% ethanol solution and scanned using micro-computed tomography (μCT40, Scanco Medical). The μCT settings were calibrated to yield a resolution of 18 μm per slice at 70 kVp and 114 μA. Subsequently, the data were transferred in DICOM format to an image-segmentation software (Amira, version 6.3.2, Thermo Fischer Scientific) for 3D reconstruction. A consistent region of interest was established across all defects by demarcating the defect margins. Within the software, specific materials and structures were differentiated based on contrast opacity or Hounsfield units, including bone, membrane, and metal fixation devices (Figs 3 and 4). For accurate assessment of the 3D structures, a virtual slice technique was employed, wherein a 2D sagittal transection was acquired. This technique facilitated the adjustment of imaging parameters to

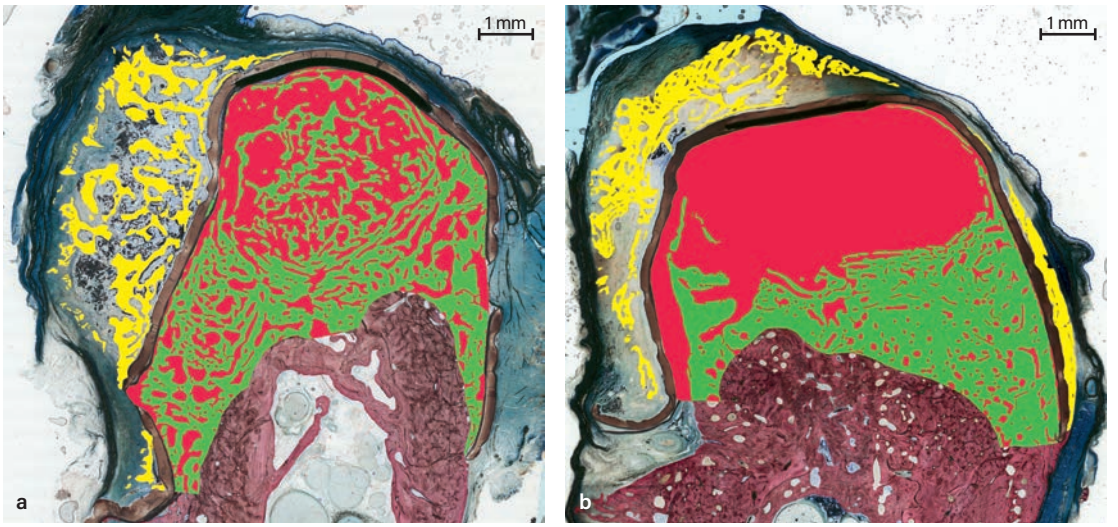

▲ **Fig 5** *(a and b)* Representative histomorphometric area analysis of the defect sites in perforated and nonperforated groups, respectively, showing bone under the membrane *(green)*, bone above the membrane *(yellow)*, and empty spaces and soft tissues *(red)*.

minimize artifact and noise, thereby enhancing the visibility of newly regenerated bone followed by image segmentation. It is pertinent to mention that metallic fixation devices exhibit a greater radiopacity relative to the surrounding bone, whereas the membranes present the lowest radiopacity.

Histologic Analysis

After μCT analysis, the specimens underwent a progressive dehydration sequence within ethanol solutions of increasing concentrations, ranging from 70% to 100%. Following dehydration, samples were embedded in a methacrylate-based resin. This was followed by cutting the blocks into sections ~300 μm thick in the buccolingual direction using a high-precision diamond blade saw (Isomet 2000, Buehler). The sections were then affixed to acrylic plates using a cyanoacrylate-based adhesive (Loctite 408, Henkel Adhesives) and allowed to set for 24 hours prior to grinding and polishing. The thickness of the sections were reduced to ~80 μm by applying a graded series of silicon carbide abrasive papers (400, 600, 800, and 1,200; Buehler) on a grinding/polishing machine (Metaserv 3000, Buehler) while ensuring continuous irrigation with water. Subsequently, sections were treated with a stain composed of Stevenel's Blue and Van Gieson's Picrofuchsin (SVG) and were then digitized via an automated slide scanning device and specialized software (Aperio CS2, Leica).[36,37] Stevenel's blue stained the cells and extracellular structures in a subtle gradation of blue tones. The counterstain, SVG, stained collagen fibers as green or greenish blue; bone as orange or purple; osteoid as yellow-green; and muscle fibers as blue to blue-green. This staining combination permitted the differentiation between the soft, connective, osteoid, and mineralized tissues.

The high-resolution digital scans were imported into Photoshop (Adobe) to quantify the area filled by tissue below and above the membrane. All scans were analyzed to identify the margins of the defect, and then color selectors were used to highlight bone (green) and soft tissue (red) below the membrane and bone above the membrane (yellow) (Fig 5). The total area of each of the colored regions was quantified using a custom computer software (JV Analysis, Biomaterials Division, New York University; Department of Biochemistry and Molecular Biology, University of Miami). The measured variables included the percentages of regenerated bone below the membrane (%RBbM), regenerated bone above the membrane (%RBaM), total regenerated bone (%TRB), and soft tissue below the membrane (%STbM). Analyses were performed by two blinded, independent investigators (N.M. and V.V.N.).

The vertical linear parameters were measured using the histologic sections corresponding to the most central aspect of the defect (along the anterioposterior direction) and closest to the tenting screws to record the maximum height of the regenerated area. Aperio ImageScope (Leica Biosystems) was used to quantify the following distances: the maximum regenerated bone height (mRBH) below the membrane (mRBHbM) and above the membrane (mRBHaM) and the total regenerated bone height (TRBH). The mRBHbM was measured as the distance between the inner point of the membrane and the outer surface of the native mandibular bone. The histologic characteristics of a lamellar bone, still maturing in the regenerating area at 8 weeks, allowed its distinction from native woven bone. The mRBHaM was evaluated as the distance between the external membrane surface and the top of the soft tissue above the membrane. TRBH is derived from the sum of mRBHbM and mRBHaM. The width of the regenerated bone (WRB) was measured as the buccolingual extent of the ridge at the largest (bottom) portion of the regenerated defect.

Statistical Analysis

The primary outcome variable from histomorphometric area analysis (%TRB), other variables (namely %RBbM, %RBaM, and %STbM), and histomorphometric linear measurements (including mRBHbM, mRBHaM, TRBH, and WRB) were compared through independent-samples *t* tests between perforated and nonperforated groups. Statistical data were presented as means and standard deviations. Statistical analyses were performed using SPSS (version 29, IBM). $P < .05$ was considered statistically significant.

Results

Surgical interventions demonstrated no complications regarding procedures, postoperative infections, and/or other clinical concerns. Additionally, upon sharp dissection of the mandible defects, there were no signs of inflammation and/or infection throughout the in vivo period.

Qualitative Volumetric Reconstruction

Three-dimensional reconstruction of the perforated group showed the distinct presence of pores on the membrane surface (Figs 3a and 3b), while the nonperforated group (Figs 3c and 3d) showed no such discontinuities at 8 weeks. From a superior-inferior view (Fig 4), both groups exhibited bone growth over the membrane, extending across the defect length (anterior to posterior direction, along the sagittal plane). Regardless of the treatment group, tenting screws, fixation screws, and reinforcement mesh were visible and intact, with no indications of loosening or displacement during the healing process.

Qualitative Histologic Evaluation

Below the membrane

Defect sites in the perforated group (Fig 6a) presented extensive bone formation characterized by the presence of high cellular content along with newly formed vasculature, as demonstrated by the extensive woven bone content at the periphery of the defect (Fig 6b). An increased degree of Haversian-like systems with lamellar reorganization was observed near the native bone, demonstrating the progressive maturation of newly formed bone (Fig 6c). In contrast, bone regeneration in the nonperforated group (Fig 7a) occurred to a lesser extent and was primarily limited to space adjacent to the native bone defect margins within the membrane confinement. The occurrence of mineralized tissue formation in close proximity to the native bone, along with the formation of newly forming vascular structures, was present in this group (Fig 7b). In the perforated group (Fig 8), soft tissue infiltration from the adjacent connective tissues was observed, albeit minimally, near membranous pores and at the defect periphery. In contrast, such soft tissue presence was more extensive in the nonperforated group defect (Fig 9), which was likely a contributing factor in the lower amounts of new bone formation.

Above the membrane

The membrane/bone interface of both groups presented a combination of direct contact between membrane and bone (Fig 10a), indicating the membrane's osteoconductive potential, and regions with soft tissue abutment (Fig 10b).

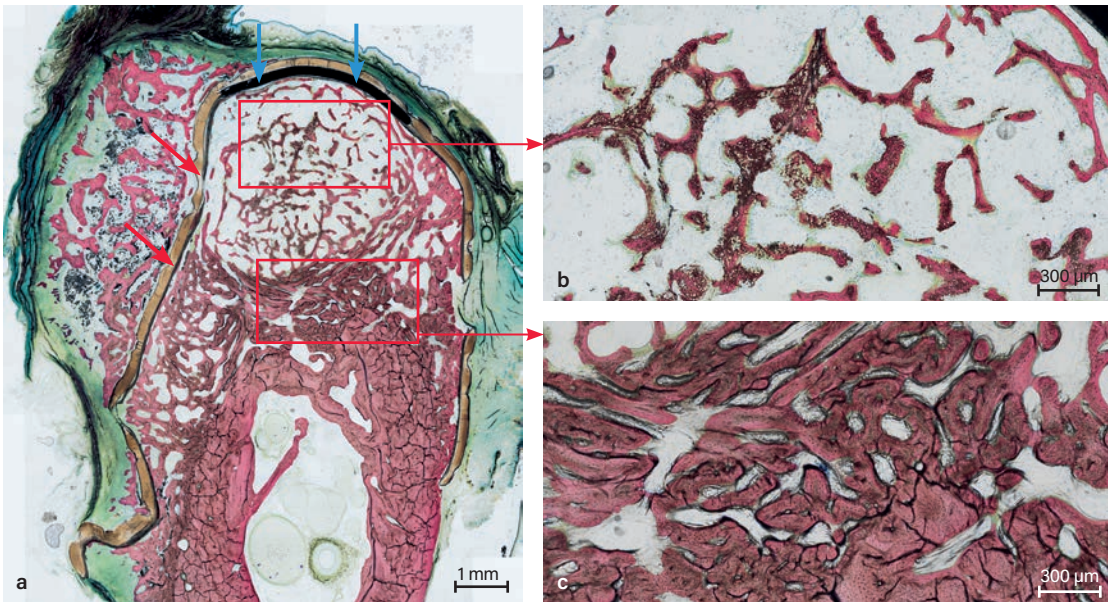

▲ **Fig 6** *(a)* Representative histomicrograph after 8 weeks of healing in the perforated group treated with a perforated PTFE membrane *(red arrows)* and reinforced with a titanium mesh *(blue arrows)*. *(b)* A magnified region of interest shows immature woven bone formation within the membrane. *(c)* A magnified region of interest shows maturing lamellar bone near the native bone margin. SVG stained the bone structures in red and stained the collagen fibers within connective/soft tissue in blue-green.

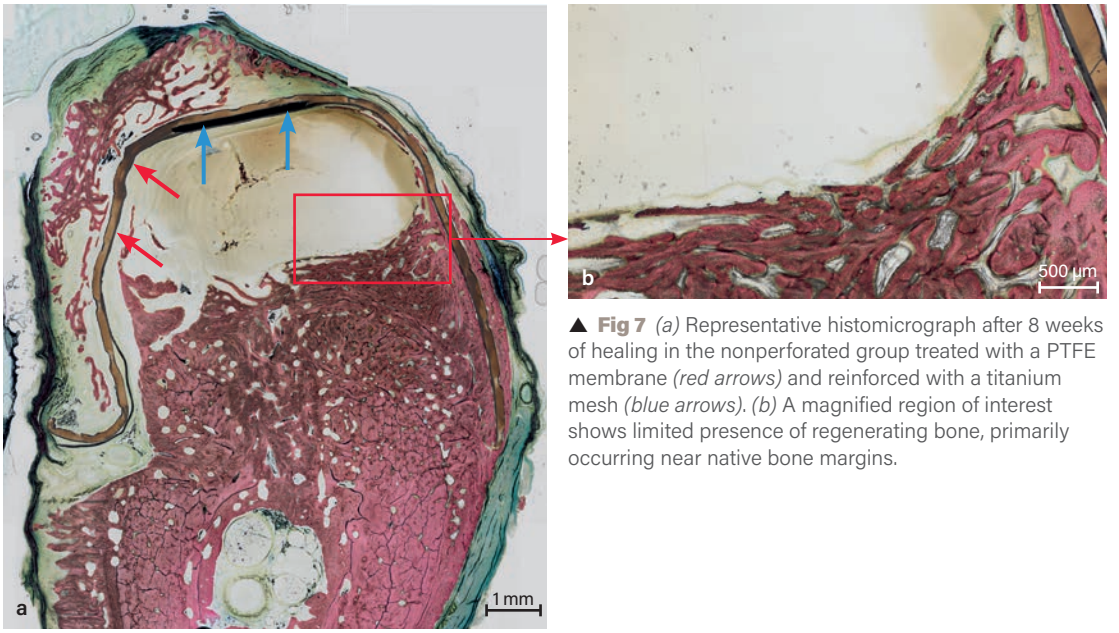

▲ **Fig 7** *(a)* Representative histomicrograph after 8 weeks of healing in the nonperforated group treated with a PTFE membrane *(red arrows)* and reinforced with a titanium mesh *(blue arrows)*. *(b)* A magnified region of interest shows limited presence of regenerating bone, primarily occurring near native bone margins.

The membrane/soft tissue interface was primarily composed of fibrovascular connective tissue with mild evidence of inflammation.

At the perforation interface

Upon a magnified examination of perforation interfaces, bone formation appeared continuous between the outside and inside of the membrane. This new bone was characterized by a stage of immature reorganization similar to the bone within the membrane (Fig 10c). The nonperforated group (Fig 10d) demonstrated no evidence of membrane disruption at 8 weeks. The majority of ectopic bone growth along the membrane was characterized

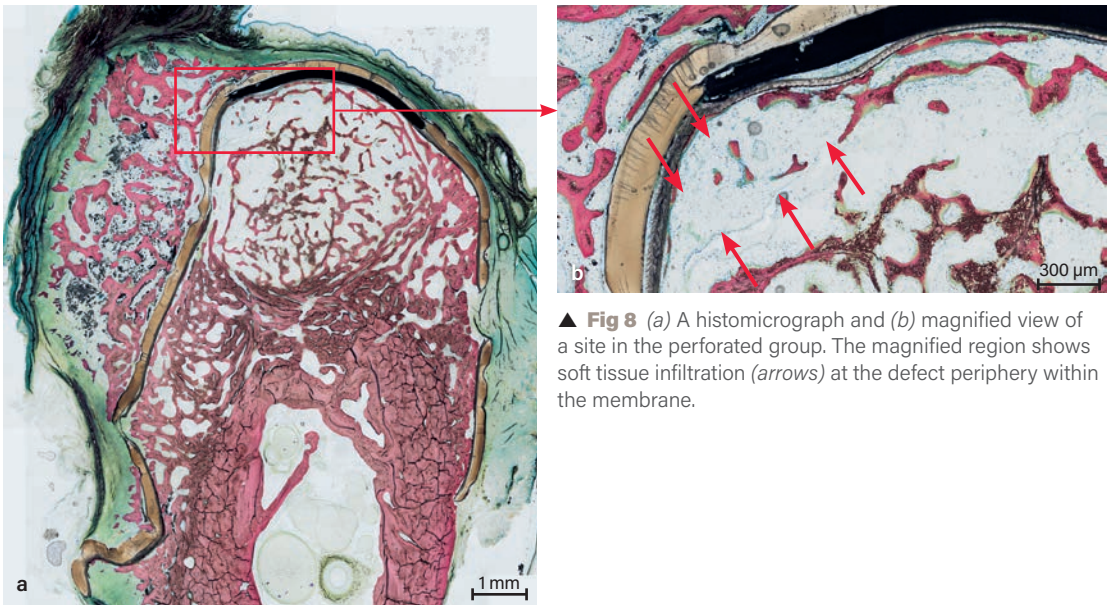

▲ **Fig 8** *(a)* A histomicrograph and *(b)* magnified view of a site in the perforated group. The magnified region shows soft tissue infiltration *(arrows)* at the defect periphery within the membrane.

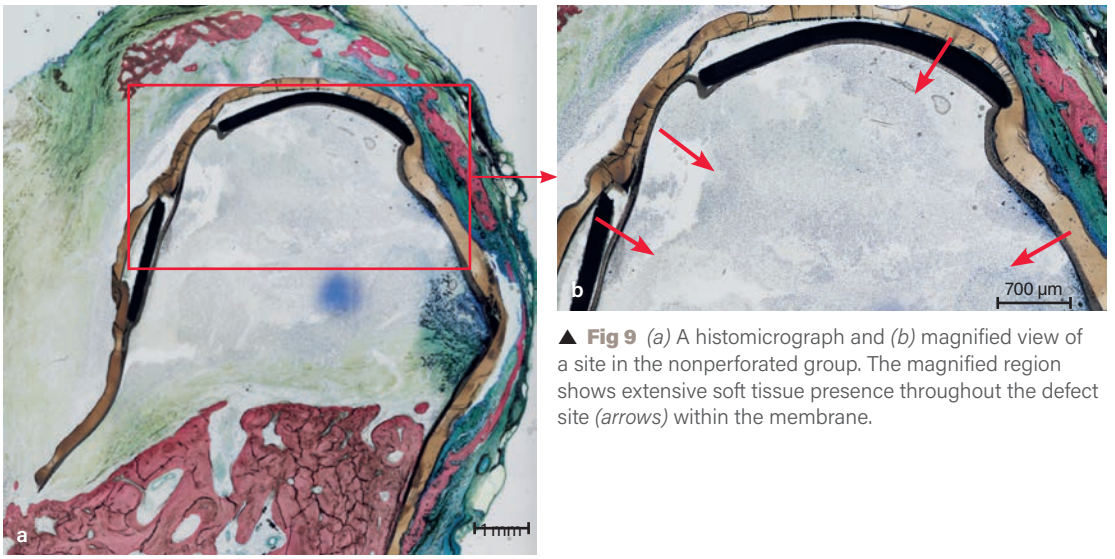

▲ **Fig 9** *(a)* A histomicrograph and *(b)* magnified view of a site in the nonperforated group. The magnified region shows extensive soft tissue presence throughout the defect site *(arrows)* within the membrane.

by a pattern of immature woven and vascularized lamellar bone, with areas of mature organization near the defect periphery, independent of the membrane group (Fig 11).

Histomorphometric Evaluation

At 8 weeks, the %RBbM was 35.19% ± 2.53% of the area, while the sites treated with nonperforated membranes showed a statistically homogenous %RBbM outcome of 14.19% ± 13.45% in the same area (P = .057) (Table 1 and Fig 12). This was accompanied by increased %STbM levels in the nonperforated group (74.82% ± 22.44%; P = .036) and decreased %STbM levels in the perforated group (32.91% ± 6.86; P = .036). The %RBaM was similar between the perforated and nonperforated groups (P = .059). Further, %TRB was significantly higher in the perforated group than the nonperforated group (67.08% ± 6.86% and 25.18% ± 22.44%, respectively; P = .036). This data reveals a reciprocal relationship: As new bone formation increases, there is a concurrent decrease in soft tissue infiltration. This phenomenon is exemplified through the analysis of porous membrane specimens and substantiates qualitative histologic observations.

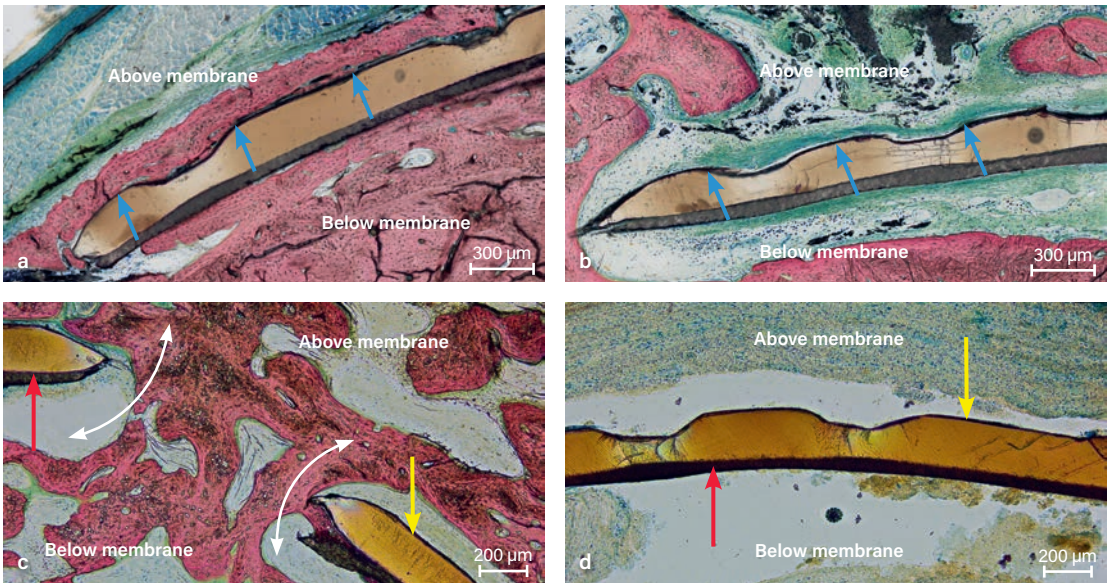

▲ **Fig 10** Representative histomicrographs at higher magnifications. Regardless of the treatment group, *(a)* the PTFE membrane surfaces were in direct contact with the regenerating bone *(arrows)* and *(b)* in intimate contact with surrounding connective tissue *(arrows)*. *(c)* The inner *(red arrows)* and outer *(yellow arrows)* surfaces of the PTFE membrane in the perforated group. The *white lines* demarcate the direction of bone regeneration between the inside and outside of the membrane. *(d)* The inner *(red arrow)* and outer *(yellow arrow)* surfaces of the PTFE membrane in the nonperforated group.

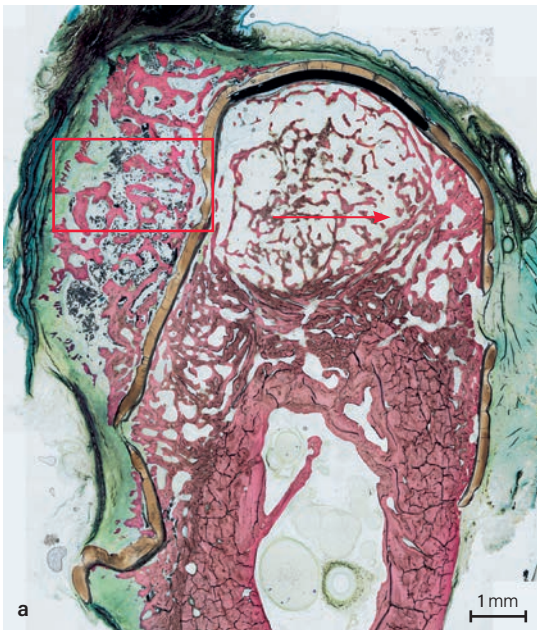

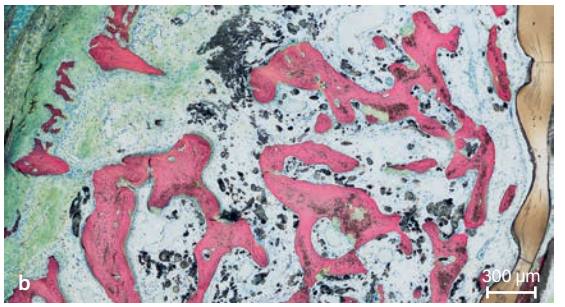

▲ **Fig 11** *(a)* A histomicrograph and *(b)* magnified view of a site in the perforated group. The magnified region of interest shows regenerating bone characteristics outside of the membrane.

Between the perforated and nonperforated groups, the mRBHaM, mRBHbM, and TRBH at 8 weeks presented statistically similar results ($P = .595$, $P = .200$, and $P = .172$, respectively). A similar trend was observed for WRB measurements as a function of treatment groups ($P = .063$) (Table 2 and Fig 13).

Discussion

The study aimed to investigate the role of the periosteum in GBR therapy of critical vertical defects in dogs with the use of rhBMP-2, delivered utilizing an ACS carrier, in both perforated and

Table 1 Histomorphometric Analysis Results: Measurements of Area

Group	RBbM	RBaM	TRB	STbM
Perforated	35.19% ± 2.53%	31.89% ± 8.66%	67.08% ± 6.86%	32.91% ± 6.86%
Nonperforated	14.19% ± 13.45%	10.98% ± 10.81%	25.18% ± 22.44%	74.82% ± 22.44%

Data are presented as mean ± SD.

▶ **Fig 12** Mean histomorphometric analysis results from %RBbM, %RBaM, %TRB, and %STbM analyses. Standard deviations are represented by error bars. Same letters denote statistically homogenous groups ($P > .05$).

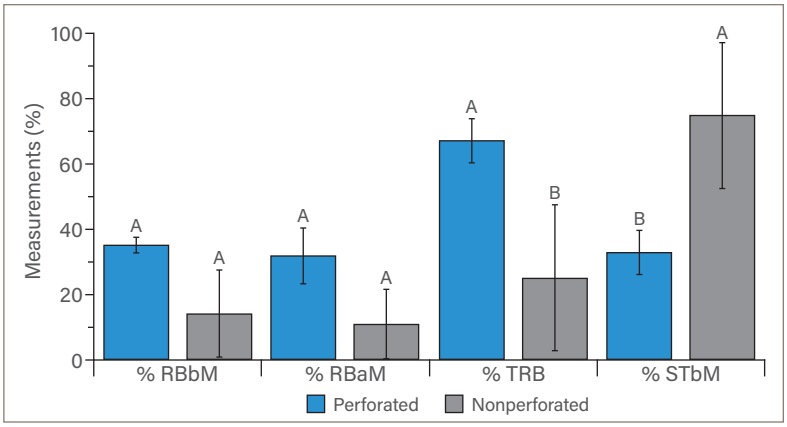

Table 2 Linear Histomorphometric Analysis Results

Group	mRBHbM	mRBHaM	TRBH	WRB
Perforated	4.66 ± 0.25 mm	4.03 ± 2.25 mm	8.69 ± 2.51 mm	3.00 ± 0.58 mm
Nonperforated	1.46 ± 0.17 mm	0.96 ± 0.92 mm	2.42 ± 0.89 mm	0.40 ± 2.03 mm

Data are presented as mean ± SD.

▶ **Fig 13** Mean histomorphometric analysis results from mRBHbM, mRBHaM, TRBH, and WRB analyses. Standard deviations are represented by error bars. Same letters denote statistically homogenous groups ($P > .05$).

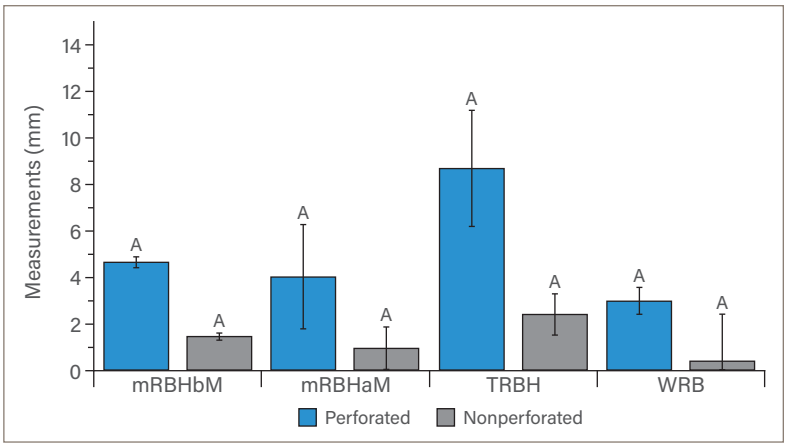

nonperforated membranes. The results support the principle that the presence of perforations (porosity) in the membrane could enhance the interaction of rhBMP-2 with the flap periosteum, thereby enhancing the regenerative processes. A previous study by Tsuji et al[27] revealed a greater therapeutic potential of rhBMP-2 in the presence of periosteal tissue. Activation of periosteum-derived progenitor cells resulted in accelerated osteogenesis and marked induction of angiogenesis, which promoted uncomplicated vascularization of the regenerating area.[27] As reported by the quantitative analysis of the present study, ~35% of the area below the perforated membrane is

represented by newly formed bone; in contrast, this value was ~15% of the area below the non-perforated membrane. Further, histologic observations demonstrated the intraporous facilitation of bony regeneration. Therefore, the perforations in the perforated group may have contributed to diffusion of rhBMP-2 through the membrane, allowing for indirect contact of the regenerating area with the periosteum. This principle ensures an essential supply of blood, oxygen, and growth factors to the tissues, improving its regenerative capacity. In both groups, ACS was used as a carrier of rhBMP-2, ensuring adequate diffusion through pores and activity with surrounding tissues.

As reported by Sanz et al, ACS can be used as an effective carrier to deliver rhBMP-2 during different surgical procedures (eg, ridge preservation or sinus augmentation).[38] Further, several histologic studies have demonstrated that the combination of rhBMP-2/ACS and osteoconductive grafts during GBR is comparable to the combination of autologous bone with titanium mesh or deproteinized bovine bone mineral.[39,40] However, to the best of the present authors' knowledge, no studies have been conducted evaluating the efficacy of rhBMP-2/ACS and perforated membranes in vertical ridge augmentation. Yet, several findings can certainly corroborate the rationale and results of the current study.

For example, a study by Zellin et al evaluated the efficacy of recombinant human transforming growth factor-1 (rhTGF-1) delivered via ACS or bioabsorbable poly(D,L-lactide-co-glycolide) (PLA/PGA) beads alone or in association with a membrane in the regeneration of transosseous defects in rat mandibles.[41] Those histologic results surprisingly showed that occlusive membrane placement significantly hampered the osteoinductive capacity of the TGF due to the lack of interaction with the periosteum.[41] All defects treated with rhTGF-1 without membrane were filled by new bone after 12 days, and bone growth outside the original defect was also observed; in sites treated with a membrane and rhTGF-1, complete filling of the defect area was reported after only 24 days.[41] Similarly, a study by Cochran et al observed delayed new bone formation in experimental canine peri-implant defects treated in combination with rhBMP-2/ACS and e-PTFE membrane, compared to defects that were treated with solely rhBMP-2/ACS.[42] The present study investigated the beneficial properties of a non-occlusive membrane conjugated with rhBMP-2 in GBR, and the findings are consistent with the mechanism of action of BMPs.

The present study's findings are in agreement with the results of other studies,[12,16] specifically in regards to the significantly lower soft tissue ingrowth within the defect area observed with the macroporous meshes. While an ideal membrane pore size has not yet been defined, a study by Aristodemou et al induced critical calvaria defects in rats with experimental diabetes, and the defects were treated with e-PTFE occlusive membranes or e-PTFE membranes with 0.5-mm holes.[16] When perforated membranes were utilized, the regenerative potential of bone tissue in rats with uncontrolled diabetes was similar to that of healthy rats and rats with controlled diabetes.[16] It was hypothesized that the creation of a partially secluded chamber allowed for the migration of osteogenic cell populations from the adjacent supracalvarian tissues (including the periosteum).[16] Additionally, a canine study by Gutta et al observed significantly greater bone growth in defects covered with a macroporous titanium mesh (pores with 1.2-mm diameters), compared to microporous (0.6-mm diameters) titanium mesh or resorbable membranes.[12] It is important to note that the inner cambium layer of the periosteum is rich in osteogenic precursor cells as well as the number of multipotent mesenchymal cells that differentiate into osteoblasts.[43] Therefore, the permeability of the membrane macropores allowed the periosteal precursor cells greater accessibility to BMP-2, thereby accelerating their differentiation into mature bone-forming cells. These findings highlight factors associated with the stimulation of new bone formation, corroborating the present results.

It is also important to highlight the limitations of the present study. The animals used herein were 3 years old and had reached skeletal maturity,[44] but it has been found that periodontal tissue regeneration is extensive in younger canines relative to medium- to older-age dogs.[45] As such, it is a goal

to conduct future studies on older cohorts to better understand how the age of the animal model affects periodontal tissue regeneration using this treatment modality. Further, randomized controlled trials are needed to confirm the trends highlighted by the present research. In vivo preclinical animal models are essential before human trials; however, they do not perfectly recreate human oral conditions and biologic healing processes. Understanding the limitations of these models is critical for prudent interpretation of preclinical findings.[46] Furthermore, a small sample size was utilized in this study, necessitating larger sample sizes for future research on this topic. Finally, a more complete histomorphometric analysis is warranted, potentially with the use of fluorescent bone markers, to more precisely demarcate the boundary between native bone and newly regenerated bone.

Conclusions

This study provides significant insights into the efficacy of perforated membranes in GBR, particularly when used in conjunction with ACS and rhBMP-2. The enhanced bone regeneration observed in the perforated group may be attributed to the increased porosity of the perforated membranes, potentially facilitating better periosteal interaction and cell migration, thereby improving the outcomes of GBR procedures. This research not only contributes to the evolving understanding of GBR techniques but also opens avenues for future studies to further optimize and refine bone regeneration strategies.

Acknowledgments

The authors declare no conflicts of interest.

References

1. Retzepi M, Donos N. Guided bone regeneration: Biological principle and therapeutic applications. Clin Oral Implants Res 2010;21:567–576.
2. Buser D, Ruskin J, Higginbottom F, Hardwick R, Dahlin C, Schenk RK. Osseointegration of titanium implants in bone regenerated in membrane-protected defects: A histologic study in the canine mandible. Int J Oral Maxillofac Implants 1995;10:666–681.
3. Dahlin C, Linde A, Gottlow J, Nyman S. Healing of bone defects by guided tissue regeneration. Plast Reconstr Surg 1988;81:672–676.
4. Dahlin C, Sennerby L, Lekholm U, Linde A, Nyman S. Generation of new bone around titanium implants using a membrane technique: An experimental study in rabbits. Int J Oral Maxillofac Implants 1989;4:19–25.
5. Schenk RK, Buser D, Hardwick WR, Dahlin C. Healing pattern of bone regeneration in membrane-protected defects: A histologic study in the canine mandible. Int J Oral Maxillofac Implants 1994;9:13–29.
6. Urban IA, Monje A. Guided bone regeneration in alveolar bone reconstruction. Oral Maxillofac Surg Clin North Am 2019;31:331–338.
7. Nyman S. Bone regeneration using the principle of guided tissue regeneration. J Clin Periodontol 1991;18:494–498.
8. Schmid J, Hammerle CH, Olah AJ, Lang NP. Membrane permeability is unnecessary for guided generation of new bone. An experimental study in the rabbit. Clin Oral Implants Res 1994;5:125–130.
9. Wang HL, Boyapati L. "PASS" principles for predictable bone regeneration. Implant Dent 2006;15:8–17.
10. Jung RE, Fenner N, Hammerle CH, Zitzmann NU. Long-term outcome of implants placed with guided bone regeneration (GBR) using resorbable and non-resorbable membranes after 12–14 years. Clin Oral Implants Res 2013;24:1065–1073.
11. Urban IA, Monje A, Lozada J, Wang HL. Principles for vertical ridge augmentation in the atrophic posterior mandible: A technical review. Int J Periodontics Restorative Dent 2017;37:639–645.
12. Gutta R, Baker RA, Bartolucci AA, Louis PJ. Barrier membranes used for ridge augmentation: Is there an optimal pore size? J Oral Maxillofac Surg 2009;67:1218–1225.
13. Hasegawa H, Masui S, Ishihata H, et al. Evaluation of a newly designed microperforated pure titanium membrane for guided bone regeneration. Int J Oral Maxillofac Implants 2019;34:411–422.
14. Mardas N, Kostopoulos L, Stavropoulos A, Karring T. Evaluation of a cell-permeable barrier for guided tissue regeneration combined with demineralized bone matrix. Clin Oral Implants Res 2003;14:812–818.
15. Simian M, Dahlin C, Blair K, Schenk RK. Effect of different microstructures of e-PTFE membranes on bone regeneration and soft tissue response: A histologic study in canine mandible. Clin Oral Implants Res 1999;10:73–84.
16. Aristodemou E, Retzepi M, Calciolari E, Donos N. The effect of experimental diabetes and membrane occlusiveness on guided bone regeneration: A proof of principle study. Clin Oral Investig 2022;26:5223–5235.
17. Dimitriou R, Mataliotakis GI, Calori GM, Giannoudis PV. The role of barrier membranes for guided bone regeneration and restoration of large bone defects: Current experimental and clinical evidence. BMC Med 2012;10:81.
18. Dreyer CH, Kjaergaard K, Ding M, Qin L. Vascular endothelial growth factor for in vivo bone formation: A systematic review. J Orthop Translat 2020;24:46–57.
19. Okuda K, Kawase T, Nagata M, et al. Tissue-engineered cultured periosteum sheet application to treat infrabony defects: Case series and 5-year results. Int J Periodontics Restorative Dent 2013;33:281–287.
20. Zhuang Z, John JV, Liao H, et al. Periosteum mimetic coating on structural bone allografts via electrospray deposition enhances repair and reconstruction of segmental defects. ACS Biomater Sci Eng 2020;6:6241–6252.

21. Lin Z, Fateh A, Salem DM, Intini G. Periosteum: Biology and applications in craniofacial bone regeneration. J Dent Res 2014;93:109–116.
22. Colnot C. Skeletal cell fate decisions within periosteum and bone marrow during bone regeneration. J Bone Miner Res 2009;24:274–282.
23. Colnot C, Zhang X, Knothe Tate ML. Current insights on the regenerative potential of the periosteum: Molecular, cellular, and endogenous engineering approaches. J Orthop Res 2012;30:1869–1878.
24. Knothe Tate ML, Ritzman TF, Schneider E, Knothe UR. Testing of a new one-stage bone-transport surgical procedure exploiting the periosteum for the repair of long-bone defects. J Bone Joint Surg Am 2007;89:307–316.
25. Knothe Tate ML, Steck R, Anderson EJ. Bone as an inspiration for a novel class of mechanoactive materials. Biomaterials 2009;30:133–140.
26. Pranskunas M, Simoliunas E, Alksne M, et al. Assessment of the bone healing process mediated by periosteum-derived mesenchymal stem cells' secretome and a xenogenic bioceramic—An in vivo study in the rabbit critical size calvarial defect model. Materials (Basel) 2021;14:3512.
27. Tsuji K, Bandyopadhyay A, Harfe BD, et al. BMP2 activity, although dispensable for bone formation, is required for the initiation of fracture healing. Nat Genet 2006;38:1424–1429.
28. Yu YY, Lieu S, Lu C, Colnot C. Bone morphogenetic protein 2 stimulates endochondral ossification by regulating periosteal cell fate during bone repair. Bone 2010;47:65–73.
29. Cray J Jr, Henderson SE, Smith DM, et al. BMP-2–regenerated calvarial bone: A biomechanical appraisal in a large animal model. Ann Plast Surg 2014;73:591–597.
30. Stokovic N, Ivanjko N, Maticic D, Luyten FP, Vukicevic S. Bone morphogenetic proteins, carriers, and animal models in the development of novel bone regenerative therapies. Materials (Basel) 2021;14:3513.
31. Jovanovic SA, Hunt DR, Bernard GW, Spiekermann H, Wozney JM, Wikesjo UM. Bone reconstruction following implantation of rhBMP-2 and guided bone regeneration in canine alveolar ridge defects. Clin Oral Implants Res 2007;18:224–230.
32. Polo CI, Lima JL, De Lucca L, et al. Effect of recombinant human bone morphogenetic protein 2 associated with a variety of bone substitutes on vertical guided bone regeneration in rabbit calvarium. J Periodontol 2013;84:360–370.
33. Wikesjo UM, Qahash M, Thomson RC, et al. rhBMP-2 significantly enhances guided bone regeneration. Clin Oral Implants Res 2004;15:194–204.
34. Zellin G, Linde A. Importance of delivery systems for growth-stimulatory factors in combination with osteopromotive membranes. An experimental study using rhBMP-2 in rat mandibular defects. J Biomed Mater Res 1997;35:181–190.
35. Hur Y, Bui MN, Griffin TJ, Ogata Y. Modified periosteal releasing incision for flap advancement: A practical technique for tensionless closure. Clin Adv Periodontics 2015;5:229–234.
36. Ramalho I, Bergamo E, Lopes A, et al. Periodontal tissue regeneration using brain-derived neurotrophic factor delivered by collagen sponge. Tissue Eng Part A 2019;25:1072–1083.
37. Tovar N, Witek L, Neiva R, et al. In vivo evaluation of resorbable supercritical CO(2)–treated collagen membranes for class III furcation-guided tissue regeneration. J Biomed Mater Res B Appl Biomater 2019;107:1320–1328.
38. Sanz M, Dahlin C, Apatzidou D, et al. Biomaterials and regenerative technologies used in bone regeneration in the craniomaxillofacial region: Consensus report of group 2 of the 15th European Workshop on Periodontology on Bone Regeneration. J Clin Periodontol 2019;46:82–91.
39. Elgali I, Omar O, Dahlin C, Thomsen P. Guided bone regeneration: Materials and biological mechanisms revisited. Eur J Oral Sci 2017;125:315–337.
40. Donos N, Dereka X, Calciolari E. The use of bioactive factors to enhance bone regeneration: A narrative review. J Clin Periodontol 2019;46:124–161.
41. Zellin G, Beck S, Hardwick R, Linde A. Opposite Effects of recombinant human transforming growth factor-β1 on bone regeneration in vivo: Effects of exclusion of periosteal cells by microporous membrane. Bone 1998;22:613–620.
42. Cochran DL, Schenk R, Buser D, Wozney JM, Jones AA. Recombinant human bone morphogenetic protein-2 stimulation of bone formation around endosseous dental implants. J Periodontol 1999;70:139–150.
43. Rosales-Rocabado JM, Kaku M, Kitami M, Akiba Y, Uoshima K. Osteoblastic differentiation and mineralization ability of periosteum-derived cells compared with bone marrow and calvaria-derived cells. J Oral Maxillofac Surg 2014;72:694.e691–699.
44. Bigham-Sadegh A, Oryan A. Selection of animal models for pre-clinical strategies in evaluating the fracture healing, bone graft substitutes and bone tissue regeneration and engineering. Connect Tissue Res 2015;56:175–194.
45. Iohara K, Murakami M, Nakata K, Nakashima M. Age-dependent decline in dental pulp regeneration after pulpectomy in dogs. Exp Gerontol 2014;52:39–45.
46. Stavropoulos A, Sculean A, Bosshardt DD, Buser D, Klinge B. Pre-clinical in vivo models for the screening of bone biomaterials for oral/craniofacial indications: Focus on small-animal models. Periodontol 2000 2015;68:55–65.

Istvan A. Urban, DMD, MD, PhD
Graduate Implant Dentistry, Loma Linda University, Loma Linda, California, USA; Urban Regeneration Institute, Budapest, Hungary.

Nicholas Mirsky, BS
Department of Biochemistry and Molecular Biology, University of Miami Miller School of Medicine, Miami, Florida, USA.

Matteo Serroni, DDS, MS
Department of Innovative Technologies in Medicine and Dentistry, University 'G. D'Annunzio' Chieti-Pescara, Chieti-Pescara, Italy.

Nick Tovar, PhD, DDS
Department of Oral and Maxillofacial Surgery, New York University Langone Medical Center and Bellevue Hospital Center, New York, New York, USA.

Vasudev Vivekanand Nayak, MSci, PhD
Department of Biochemistry and Molecular Biology, University of Miami Miller School of Medicine, Miami, Florida, USA; Dr. John T. Macdonald Foundation Biomedical Nanotechnology Institute (BioNIUM), University of Miami, Miami, Florida, USA.

Lukasz Witek, MSci, PhD
Biomaterials and Regenerative Biology Division, New York University College of Dentistry, New York, New York, USA; Department of Biomedical Engineering, New York University Tandon School of Engineering, Brooklyn, New York, USA; Hansjörg Wyss Department of Plastic Surgery, New York University Grossman School of Medicine, New York, New York, USA.

Charles Marin, DDS, MS, PhD
Universidade Federal de Santa Catarina, Department of Dentistry, Division of Oral and Maxillofacial Surgery, Florianopolis, Brazil.

Muhammad H. A. Saleh, BDS, MS, MSD
Department of Periodontics and Oral Medicine, University of Michigan School of Dentistry, Ann Arbor, Michigan, USA.

Andrea Ravidà, DDS, MS, PhD
Department of Periodontics and Preventive Dentistry, University of Pittsburgh School of Dental Medicine, Pittsburgh, Pennsylvania, USA.

Istvan Baczko, MD, PhD
Department of Pharmacology and Pharmacotherapy, Albert Szent-Györgyi Medical School, University of Szeged, Szeged, Hungary.

Laszlo Parkanyi, DDS, PhD
Department of Oral Surgery, University of Szeged, Faculty of Dentistry, Szeged, Hungary.

Katalin Nagy, DDS, PhD
Department of Periodontology, University of Szeged, Faculty of Dentistry, Szeged, Hungary.

Paulo G. Coelho, MD, DDS, PhD, MBA
Department of Biochemistry and Molecular Biology, University of Miami Miller School of Medicine, Miami, Florida, USA; Dr. John T. Macdonald Foundation Biomedical Nanotechnology Institute (BioNIUM), University of Miami, Miami, Florida, USA; DeWitt Daughtry Family Department of Surgery, Division of Plastic Surgery, University of Miami Miller School of Medicine, Miami, Florida, USA.

Correspondence to:
Dr Vasudev Vivekanand Nayak, vxn188@miami.edu